Modern Adaptation of Prandtl's Classic Lifting-Line Theory

W. F. Phillips* and D. O. Snyder†
Utah State University, Logan, Utah 84322-4130

The classical solution to Prandtl's well-known lifting-line theory applies only to a single lifting surface with no sweep and no dihedral. However, Prandtl's original model of a finite lifting surface has much broader applicability. A general numerical lifting-line method based on Prandtl's model is presented. Whereas classical lifting-line theory is based on applying the two-dimensional Kutta–Joukowski law to a three-dimensional flow, the present method is based on a fully three-dimensional vortex lifting law. The method can be used for systems of lifting surfaces with arbitrary camber, sweep, and dihedral. The accuracy realized from this method is shown to be comparable to that obtained from numerical panel methods and inviscid computational fluid dynamics solutions, but at a small fraction of the computational cost.

Nomenclature

A_r = global reference area
b = twice the lifting surface semispan
$C_{\ell i}$ = section lift coefficient for wing section i
$C_{\ell \alpha}$ = airfoil section lift slope
$C_{\ell \alpha i}$ = section lift slope for wing section i
$C_{\ell \infty}$ = section lift coefficient for an infinite wing
C_{mi} = section moment coefficient for wing section i
c = local section chord length
$\bar{c}$ = overall aerodynamic mean chord length
$\bar{c}_i$ = aerodynamic mean chord length for wing section i
dA_i = differential planform area at control point i
$\mathbf{dF}$ = differential aerodynamic force vector
$\mathbf{d\ell}$ = directed differential vortex length vector
$\mathbf{F}$ = net force exerted by fluid on the surroundings
f_{d_i} = local section induced drag per unit span
f_ℓ = local section lift per unit span
$\mathbf{G}$ = dimensionless vortex strength vector
G_i = dimensionless vortex strength for section i
$[\mathbf{J}]$ = N by N matrix of partial derivatives
L_r = global reference length
$\mathbf{M}$ = net moment about the c.g. exerted by the fluid
N = total number of horseshoe vortices
n = number of horseshoe vortices per semispan
$\mathbf{R}$ = residual vector
R_a = aspect ratio
$\mathbf{r}_i$ = vector from c.g. to control point i
$\mathbf{r}_{i_1 j}$ = vector from node $i1$ to control j
$\mathbf{r}_{i_2 j}$ = vector from node $i2$ to control j
r_1, r_2 = magnitudes of $\mathbf{r}_1$ and $\mathbf{r}_2$
$\mathbf{r}_0$ = vector from beginning to end of vortex segment
$\mathbf{r}_1$ = vector from beginning of vortex segment to arbitrary point in space
$\mathbf{r}_2$ = vector from end of vortex segment to arbitrary point in space
s = spanwise coordinate
$\mathbf{u}_{ai}$ = chordwise unit vector at control point i
$\mathbf{u}_{ni}$ = normal unit vector at control point i
$\mathbf{u}_{si}$ = spanwise unit vector at control point i
$\mathbf{u}_\infty$ = unit vector in direction of the freestream

V_∞ = magnitude of $\mathbf{V}_\infty$
$\mathbf{V}$ = local fluid velocity
$\mathbf{V}_\infty$ = velocity of the uniform flow or freestream
$\mathcal{V}$ = fluid volume
$\mathbf{v}_{ij}$ = dimensionless velocity induced at control point j by vortex i, having a unit strength
$\mathbf{v}_\infty$ = unit vector in direction of freestream
α_i = local angle of attack for wing section i
α_{L0i} = local zero-lift angle of attack with no flap deflection
Γ = vortex strength in the direction of $\mathbf{r}_0$
Γ_i = strength of horseshoe vortex i
$\Delta \mathbf{G}$ = dimensionless strength correction vector
δA_i = planform area of wing section i
δ_i = flap deflection for wing section i
$\delta \boldsymbol{\ell}_i$ = spatial vector along the bound segment i
$\delta \mathbf{M}_i$ = quarter-chord moment for wing section i
ε_i = flap effectiveness for wing section i
$\boldsymbol{\zeta}_i$ = dimensionless spanwise length vector
θ = angle from $\mathbf{r}_1$ to $\mathbf{r}_2$
ρ = fluid density
Ω = relaxation factor
ω = local fluid vorticity

Introduction

THE development of Prandtl's lifting-line theory,[1,2] provided the first analytical method for accurately predicting lift and induced drag on a finite lifting surface. In this theory, Prandtl hypothesized that each spanwise section of a finite wing has a section lift equivalent to that acting on a similar section of an infinite wing having the same section circulation. With this hypothesis, the two-dimensional vortex lifting law of Kutta[3] and Joukowski[4] was applied at each section of the three-dimensional wing, to relate the local aerodynamic force to the local circulation. However, to fix the direction of the aerodynamic force vector, the undisturbed freestream velocity in the Kutta–Joukowski law was, intuitively and without proof, replaced with the vector sum of the freestream velocity and the velocity induced by the trailing vortex sheet. This theory gives good agreement with experimental data for straight wings of aspect ratio greater than about four. Prandtl's lifting-line theory has had a profound impact on the development of modern aerodynamics and hydrodynamics and is still widely used today. However, conventional lifting-line theory applies only to a single lifting surface with no sweep and no dihedral.

In most modern textbooks (e.g., Bertin and Smith[5]), Prandtl's hypothesis is justified based on the provision that flow in the spanwise direction is small. The failure of conventional lifting-line theory to accurately predict the aerodynamic forces acting on a swept wing is usually blamed on the violation of this provision. However, it can be shown from the three-dimensional vortex lifting law that the

relationship between section lift and section circulation is not affected by flow parallel to the bound vorticity (see Saffman[6]). The three-dimensional vortex lifting law requires that, for any volume enclosed by a stream surface in an inviscid, incompressible, steady flow, a force must be exerted on the surrounding sequal to the product of the fluid density and the cross product of the local fluid velocity with the local fluid vorticity, integrated over the volume. Saffman[6] presents a proof of this vortex lifting law.

Only in the limiting case of two-dimensional potential flow can the local fluid velocity vector in the vortex lifting law be replaced with the freestream velocity. For this special case, the general vortex lifting law reduces to the two-dimensional Kutta–Joukowski law. Strictly speaking, the two-dimensional Kutta–Joukowski law cannot be used to relate section lift to section circulation in a three-dimensional potential flow. However, the three-dimensional vortex lifting law, applied to Prandtl's model of the finite wing, requires a local section lift equal to the cross product of the local fluid velocity vector with the local circulation vector, multiplied by the fluid density, $\rho(V \times \Gamma)$. This cross product results in a section lift that is independent of the component of fluid velocity that is parallel to the bound vorticity.

If the fluid flow component parallel to the bound vorticity has no effect on the section lift, why does conventional lifting-line theory fail to predict the performance of swept wings? The answer is also provided by the general vortex lifting law. When computing section lift from the general vortex lifting law, the local velocity induced on each vortex segment must include the velocity induced by the remainder of that same vortex as well as that induced by all other potentials included within the flowfield. This means that, when computing the lift on any wing section, we must include the velocity induced by all other vortex segments, free or bound, that are contained within the flowfield. In the development of classical lifting-line theory, Prandtl intuitively added the velocity induced by the trailing vortex sheet to the undisturbed freestream velocity specified by the two-dimensional Kutta–Joukowski law. However, he did not suggest including the velocity induced by one bound vortex segment on another.

For flow over a straight lifting surface, the bound vortex filaments are all reasonably parallel. For any two parallel vortex filaments, the force resulting from the velocity induced on the first filament by the second is equal, opposite, and collinear with the force resulting from the velocity induced on the second filament by the first. Thus, for straight lifting surfaces, the parallel nature of the bound vorticity makes it reasonable to neglect the interaction between bound vortex filaments and compute the section lift based only on the velocity induced by the trailing vortex sheet and the undisturbed uniform flow.

For flow over a swept wing, the bound vortex filaments on each side of the wing are roughly parallel to each other and to the local wing quarter chord. However, the bound vortex filaments on one side of the wing are not parallel to the bound vortex filaments on the other side. Thus, for a lifting swept wing, the bound vorticity generated on one side of the wing produces downwash on the other side of the wing. This downwash reduces the net lift and increases the total induced drag for the wing. The downwash resulting from the bound vorticity is greatest near the center of the wing, whereas the downwash resulting from the trailing vorticity is greatest near the wing tips. Thus, for a swept wing, the lift is reduced both near the center of the wing and near the tips.

Prandtl's classical lifting-line theory is based on a linear relationship between section lift and section angle of attack. With this linear assumption, and with the assumption of a straight lifting line, the theory provides an analytical solution for the spanwise distribution of lift and induced drag acting on a finite lifting surface. The solution is in the form of an infinite sine series for the circulation distribution. Historically, the coefficients in this sine series have usually been evaluated from collocation methods. Typically, the series is truncated to a finite series, and the coefficients in the finite series are evaluated by requiring the lifting-line equation to be satisfied at a number of spanwise locations equal to the number of terms in the series. A very straightforward method was first presented by

Glauert.[7] The most popular method, based on Gaussian quadrature, was originally presented by Multhopp.[8] Most recently, Rasmussen and Smith[9] have presented a more rigorous and more rapidly converging method, based on a Fourier series expansion similar to that first used by Lotz[10] and Karamcheti.[11]

Purely numerical methods for solving the lifting-line equation have also been proposed. McCormick[12] has presented a numerical method that can be used for a single lifting surface having a straight lifting line. This method is based on applying the two-dimensional Kutta–Joukowski law to the three-dimensional flow and neglects the downwash generated by the bound vorticity. Results obtained from this method are essentially identical to those obtained from the series solution. A numerical lifting-line method has also been developed by Anderson et al.[13] that relaxes the assumption of linearity between section lift and section angle of attack. For a single straight lifting surface, this method gives good agreement with experimental data at angles of attack both below and above stall. However, the method still assumes a straight lifting line and ignores the downwash produced by the bound vorticity. Thus, as is the case with all methods used to obtain solutions to the classical lifting-line equation, this numerical method applies only to a single lifting surface with no sweep and no dihedral.

Here, a numerical lifting-line method is presented that can be used to obtain the forces and moments acting on a system of lifting surfaces with arbitrary position and orientation. This method, based on Prandtl's original model of a finite wing, accurately predicts the effects of both sweep and dihedral as well as the effects of aspect ratio, camber, and planform shape. Results obtained from this method are compared with experimental data and with results from other numerical methods. The accuracy realized from the present method is shown to be comparable to that obtained from numerical panel methods and inviscid computational fluid dynamics (CFD) solutions, but at a small fraction of the computational cost. In addition to the obvious applications to aeronautics, this method has broad application to the field of hydrodynamics, including hydrofoils, marine propellers, and control surfaces. Unlike the classical lifting-line solution, the present method is not based on a linear relationship between section lift and section angle of attack. Thus, the method could conceivably be applied, with caution, to account approximately for the effects of stall.

Formulation

In what is commonly referred to as the numerical lifting-line method (e.g., Katz and Plotkin[14]), a finite wing is synthesized using a composite of horseshoe shaped vortices. The continuous distribution of bound vorticity over the surface of the wing, as well as the continuous distribution of free vorticity in the trailing vortex sheet, is approximated by a finite number of discrete horseshoe vortices, as shown in Fig. 1.

The bound portion of each horseshoe vortex is placed coincident with the wing quarter-chord line and is, thus, aligned with the local sweep and dihedral. The trailing portion of each horseshoe vortex is aligned with the trailing vortex sheet. The left-hand corner of one
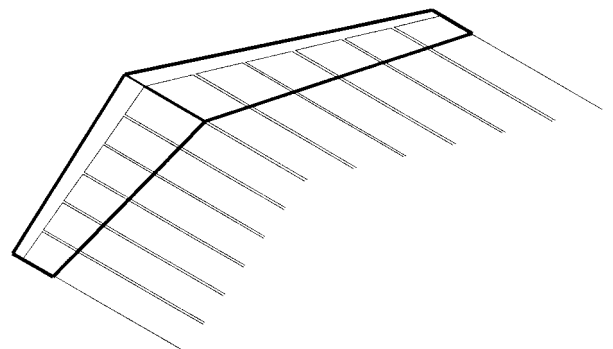

Fig. 1 Horseshoe vortices distributed along the quarter chord of a finite wing with sweep and dihedral.
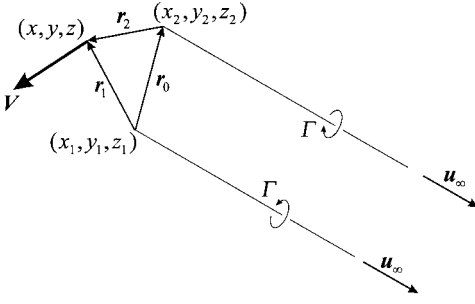
Fig. 2   Position vectors describing the geometry for a horseshoe vortex.

horseshoe and the right-hand corner of the next are placed on the same nodal point. Thus, except at the wing tips, each trailing vortex segment is coincident with another trailing segment from the adjacent vortex. If two adjacent vortices have exactly the same strength, then the two coincident trailing segments exactly cancel because one has clockwise rotation and the other has counterclockwise rotation. The net vorticity that is shed from the wing at any internal node is simply the difference in the vorticity of the two adjacent vortices that share that node.

Each horseshoe vortex is composed of three straight vortex segments. From the Biot–Savart law and the nomenclature defined in Fig. 2, the velocity vector induced at an arbitrary point in space, by any straight vortex segment, is readily found to be, for example, see Bertin and Smith[5] or Katz and Plotkin,[15]

$$V = \frac{\Gamma}{4\pi} \frac{r_1 \times r_2}{|r_1 \times r_2|^2} r_0 \cdot \left(\frac{r_1}{r_2} - \frac{r_2}{r_2} \right) \qquad (1)$$

Although Eq. (1) is in the form commonly found in modern textbooks, it is not the most useful form for numerical calculations. The induced velocity computed from Eq. (1) is indeterminate whenever r_1 and r_2 are collinear, even for points that lie outside the vortex segment. To eliminate this division by zero for points that are not on the vortex segment, we can make use of the trigonometric relations

$$r_0 = r_1 - r_2, \quad r_1 \cdot r_2 = r_1 r_2 \cos\theta, \quad |r_1 \times r_2| = r_1 r_2 \sin\theta$$

Using these relations we have

$$\frac{r_0}{|r_1 \times r_2|^2} \cdot \left(\frac{r_1}{r_1} - \frac{r_2}{r_2} \right) = \frac{r_1 - r_2}{|r_1 \times r_2|^2} \cdot \left(\frac{r_1}{r_1} - \frac{r_2}{r_2} \right)$$

$$= \frac{1}{r_1^2 r_2^2 \sin^2\theta} \left(r_1 + r_2 - \frac{r_1 \cdot r_2}{r_2} - \frac{r_1 \cdot r_2}{r_1} \right)$$

$$= \frac{(r_1 + r_2)(1 - \cos\theta)}{r_1^2 r_2^2 (1 - \cos^2\theta)} = \frac{r_1 + r_2}{r_1^2 r_2^2 (1 + \cos\theta)}$$

$$= \frac{r_1 + r_2}{r_1 r_2 (r_1 r_2 + r_1 \cdot r_2)}$$

and Eq. (1) can be more conveniently written as

$$V = \frac{\Gamma}{4\pi} \frac{(r_1 + r_2)(r_1 \times r_2)}{r_1 r_2 (r_1 r_2 + r_1 \cdot r_2)} \qquad (2)$$

Notice that, unlike the result from Eq. (1), the induced velocity computed from Eq. (2) is not singular when the angle from r_1 to r_2 is zero. It is, however, still singular when this angle is $\pm\pi$.

When we use Eq. (2) for the finite bound segment and the two semi-infinite trailing segments shown in Fig. 2, the velocity vector

induced at an arbitrary point in space, by a complete horseshoe vortex, is

$$V = \frac{\Gamma}{4\pi} \left[\frac{u_\infty \times r_2}{r_2(r_2 - u_\infty \cdot r_2)} + \frac{(r_1 + r_2)(r_1 \times r_2)}{r_1 r_2 (r_1 r_2 + r_1 \cdot r_2)} - \frac{u_\infty \times r_1}{r_1(r_1 - u_\infty \cdot r_1)} \right]$$
$$(3)$$

As is the case with panel methods, the user must specify the orientation of the trailing vortex sheet. In obtaining the classical lifting-line solution for a single lifting surface with no sweep or dihedral, Prandtl assumed the trailing vortex sheet to be aligned with the wing chord. This was done to facilitate obtaining an analytic solution. In obtaining a numerical solution, there is little advantage in aligning the trailing vortex sheet with a vehicle axis such as the chord line. More correctly, the trailing vortex sheet should be aligned with the freestream. This is done easily in the numerical solution by setting u_∞ equal to the unit vector in the direction of the freestream. Although it is intuitively more appealing to align the trailing vortex sheet with the freestream, in reality, this makes very little difference in the final result. For typical wings, aligning the trailing vortex sheet with the chord line rather than the freestream produces errors in the resulting forces and moments of less than 1%. Still, because the method allows the trailing vortex sheet to be aligned easily with the freestream, this should always be done.

When a system of lifting surfaces is synthesized using N horseshoe vortices, in a manner similar to that shown in Fig. 1, Eq. (3) can be used to determine the resultant velocity induced at any point in space, if the strength of each horseshoe vortex is known. However, these strengths are not known a priori. To compute the strengths of the N vortices, we must have a system of N equations relating these N strengths to some known properties of the wing. In what has commonly been referred to as the numerical lifting-line method,[14] these N equations are provided by forcing a Neumann condition, which specifies zero normal velocity at the three-quarter chord of the wing section midway between the trailing legs of each horseshoe vortex. This method works remarkably well for planar swept wings with no camber. However, not surprisingly, this method does not work well for cambered wings or for wings including deflected flaps and/or control surfaces.

In reality, this numerical lifting-line method is simply the vortex lattice method[16,17] applied using only a single lattice element, in the chordwise direction, for each spanwise subdivision of the wing. Applying the Neumann condition at only one point in the chordwise direction is clearly not adequate for wing sections with camber or flap deflection. This method gives a result that depends only on the position and slope of the camber line at the three-quarter chord. The predicted performance is completely independent of camber line shape at any other chordwise location. This is clearly not realistic.

For a more pragmatic approach, we turn to the general three-dimensional vortex lifting law,[6]

$$F = \iiint_\mathcal{V} \rho(V \times \omega) \, d\mathcal{V}$$

Using Prandtl's hypothesis, we assume that each spanwise wing section has a section lift equivalent to that acting on a similar section of an infinite wing with the same local angle of attack. Thus, applying the vortex lifting law to a differential segment of the lifting line, we have

$$dF = \rho \Gamma V \times d\ell \qquad (4)$$

If flow over a finite lifting surface is synthesized from a uniform flow combined with horseshoe vortices placed along the quarter-chord line, from Eq. (3), the local velocity induced at a control point placed anywhere along the bound segment of horseshoe vortex j is

$$V_j = V_\infty + \sum_{i=1}^{N} \frac{\Gamma_i v_{ij}}{\bar{c}_i} \qquad (5)$$

where v_{ij} is the dimensionless induced velocity

$$
v_{ij} \equiv
\begin{cases}
\dfrac{\bar{c}_i}{4\pi}
\left[
\dfrac{u_\infty \times r_{i_2 j}}{r_{i_2 j}\left(r_{i_2 j} - u_\infty \cdot r_{i_2 j}\right)}
+ \dfrac{\left(r_{i_1 j} + r_{i_2 j}\right)\left(r_{i_1 j} \times r_{i_2 j}\right)}{r_{i_1 j} r_{i_2 j}\left(r_{i_1 j} r_{i_2 j} + r_{i_1 j} \cdot r_{i_2 j}\right)}
- \dfrac{u_\infty \times r_{i_1 j}}{r_{i_1 j}\left(r_{i_1 j} - u_\infty \cdot r_{i_1 j}\right)}
\right], & i \neq j \\[2em]
\dfrac{\bar{c}_i}{4\pi}
\left[
\dfrac{u_\infty \times r_{i_2 j}}{r_{i_2 j}\left(r_{i_2 j} - u_\infty \cdot r_{i_2 j}\right)}
- \dfrac{u_\infty \times r_{i_1 j}}{r_{i_1 j}\left(r_{i_1 j} - u_\infty \cdot r_{i_1 j}\right)}
\right], & i = j
\end{cases}
\tag{6}
$$

At this point, $\bar{c}_i$ could be any characteristic length associated with the wing section aligned with horseshoe vortex i. This characteristic length is simply used to nondimensionalize Eq. (6) and has no effect on the induced velocity. The choice of characteristic length will be addressed later. The bound vortex segment is excluded from Eq. (6), when $i = j$, because a straight vortex segment induces no downwash along its own length.

From Eqs. (4) and (5), the aerodynamic force acting on a spanwise differential section of the lifting surface located at control point i is given by

$$
\mathbf{d}F_i = \rho \Gamma_i \left(V_\infty + \sum_{j=1}^{N} \frac{\Gamma_j}{\bar{c}_j} v_{ji} \right) \times \mathbf{d}\ell_i
\tag{7}
$$

When we allow for the possibility of flap deflection, the local section lift coefficient for the airfoil section located at control point i is a function of local angle of attack and local flap deflection,

$$
C_{\ell i} = C_{\ell i}(\alpha_i, \delta_i)
\tag{8}
$$

The local angle of attack at control point i is

$$
\alpha_i = \tan^{-1}\left(\frac{V_i \cdot u_{ni}}{V_i \cdot u_{ai}} \right)
\tag{9}
$$

where u_{ai} and u_{ni} are, respectively, the unit vectors in the chordwise direction and the direction normal to the chord, both in the plane of the local airfoil section as shown in Fig. 3. If the relation implied by Eq. (8) is known at each section of the wing, the magnitude of the aerodynamic force acting on a spanwise differential section of the wing located at control point i can be written as

$$
|\mathbf{d}F_i| = \tfrac{1}{2}\rho V_\infty^2 C_{\ell i}(\alpha_i, \delta_i)\, \mathrm{d}A_i
\tag{10}
$$

Setting the magnitude of the force from Eq. (7) equal to that obtained from Eq. (10) and rearranging, we can write

$$
2\left| \left(v_\infty + \sum_{j=1}^{N} v_{ji} G_j \right) \times \zeta_i \right| G_i - C_{\ell i}(\alpha_i, \delta_i) = 0
\tag{11}
$$

u_{ni}
quarter-chord line
horseshoe vortex i
u_{si}
u_{ai} Γ_i
u_∞
Γ_i
u_∞
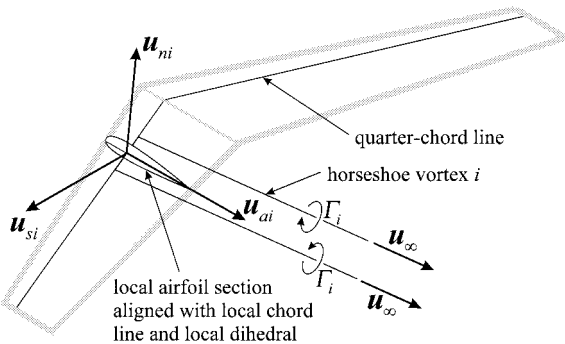local airfoil section
aligned with local chord
line and local dihedral

Fig. 3 Unit vectors describing the orientation of the local airfoil section.

where

$$
v_\infty \equiv \frac{V_\infty}{V_\infty}, \qquad \zeta_i \equiv \bar{c}_i \frac{\mathrm{d}\ell_i}{\mathrm{d}A_i}, \qquad G_i \equiv \frac{\Gamma_i}{\bar{c}_i V_\infty}
$$

and, from Eqs. (5) and (9), the local angle of attack written in terms of the dimensionless variables is given by

$$
\alpha_i = \tan^{-1}\left[\frac{\left(v_\infty + \sum_{j=1}^{N} v_{ji} G_j \right) \cdot u_{ni}}{\left(v_\infty + \sum_{j=1}^{N} v_{ji} G_j \right) \cdot u_{ai}} \right]
\tag{12}
$$

Equation (11) can be written for N different control points, one associated with each of the N horseshoe vortices used to synthesize the lifting surface or system of lifting surfaces. This provides a system of N nonlinear equations relating the N unknown dimensionless vortex strengths G_i to known properties of the wing. At angles of attack below stall, this system of nonlinear equations surrenders quickly to Newton's method.

To apply Newton's method, the system of equations is written in the vector form:

$$
\mathcal{F}(G) = R
\tag{13}
$$

where

$$
\mathcal{F}_i(G) = 2\left| \left(v_\infty + \sum_{j=1}^{N} v_{ji} G_j \right) \times \zeta_i \right| G_i - C_{\ell i}(\alpha_i, \delta_i)
\tag{14}
$$

We wish to find the vector of dimensionless vortex strengths G that makes all components of the residual vector R go to zero. Thus, we want the change in the residual vector to be $-R$. We start with an initial estimate for the G vector and iteratively refine the estimate by applying the Newton corrector equation

$$
[J]\Delta G = -R
\tag{15}
$$

where $[J]$ is the N by N matrix of partial derivatives

$$
J_{ij} = \frac{\partial \mathcal{F}_i}{\partial G_j} =
\begin{cases}
\dfrac{2 w_i \cdot (v_{ji} \times \zeta_i)}{|w_i|} G_i
- \dfrac{\partial C_{\ell i}}{\partial \alpha_i} \dfrac{v_{ai}(v_{ji} \cdot u_{ni}) - v_{ni}(v_{ji} \cdot u_{ai})}{v_{ai}^2 + v_{ni}^2}, & j \neq i \\[2em]
2|w_i| + \dfrac{2 w_i \cdot (v_{ji} \times \zeta_i)}{|w_i|} G_i
- \dfrac{\partial C_{\ell i}}{\partial \alpha_i} \dfrac{v_{ai}(v_{ji} \cdot u_{ni}) - v_{ni}(v_{ji} \cdot u_{ai})}{v_{ai}^2 + v_{ni}^2}, & j = i
\end{cases}
\tag{16}
$$

$$
w_i \equiv \left(v_\infty + \sum_{j=1}^{N} v_{ji} G_j \right) \times \zeta_i
\tag{17}
$$

$$
v_{ni} \equiv \left(v_\infty + \sum_{j=1}^{N} v_{ji} G_j \right) \cdot u_{ni}
\tag{18}
$$

and

$$
v_{ai} \equiv \left(v_\infty + \sum_{j=1}^{N} v_{ji} G_j \right) \cdot u_{ai}
\tag{19}
$$

Using Eq. (16) in Eq. (15), we compute the correction vector ΔG. This correction vector is used to obtain an improved estimate for the dimensionless vortex strength vector G according to

$$
G = G + \Omega \Delta G
\tag{20}
$$

This process is repeated until the magnitude of the largest residual is less than some convergence criteria. For angles of attack below stall, this method converges very rapidly using almost any initial estimate for G and a relaxation factor Ω of unity. At angles of attack beyond stall, the method must be highly under relaxed and is very sensitive to the initial estimate for G.

For the fastest possible convergence of Newton's method, we require an accurate initial estimate for the dimensionless vortex strength vector. For this purpose, a linearized version of Eq. (11) is useful. For a straight lifting surface of infinite aspect ratio at small angles of attack, the downwash is zero, the section lift is a linear function of angle of attack, and all nonlinear terms in Eq. (11) vanish. For a lifting surface of high aspect ratio with no sweep or dihedral, at small angles of attack, we can still ignore the nonlinear terms and compute an approximate dimensionless vortex strength vector from this linear system.

At small angles of attack, the local section lift coefficient can be approximated as

$$C_{\ell i}(\alpha_i, \delta_i) \cong C_{\ell \alpha i}(\alpha_i - \alpha_{L0i} + \varepsilon_i \delta_i) \tag{21}$$

Using the small angle approximation for both the geometric angle of attack and the induced angle of attack, after applying Eq. (12) to Eq. (21), we have

$$C_{\ell i} \cong C_{\ell \alpha i} \left(\boldsymbol{v}_\infty \cdot \boldsymbol{u}_{ni} + \sum_{j=1}^N \boldsymbol{v}_{ji} \cdot \boldsymbol{u}_{ni} G_j - \alpha_{L0i} + \varepsilon_i \delta_i \right) \tag{22}$$

Applying Eq. (22) to Eq. (11) and ignoring second-order terms, we obtain the linear system

$$2|\boldsymbol{v}_\infty \times \boldsymbol{\zeta}_i| G_i - C_{\ell \alpha i} \sum_{j=1}^N \boldsymbol{v}_{ji} \cdot \boldsymbol{u}_{ni} G_j = C_{\ell \alpha i}(\boldsymbol{v}_\infty \cdot \boldsymbol{u}_{ni} - \alpha_{L0i} + \varepsilon_i \delta_i) \tag{23}$$

Equation (23) gives good results, at small angles of attack, for a single lifting surface of high aspect ratio with no sweep or dihedral. For larger angles of attack, highly swept wings, or for interacting systems of lifting surfaces, the nonlinear system given by Eq. (11) should be used. However, Eq. (23) provides a reasonable initial estimate for the dimensionless vortex strength vector, to be used with Newton's method for obtaining a solution to this nonlinear system.

Aerodynamic Forces and Moments

Once the vortex strengths have been determined, the total aerodynamic force vector can be determined from Eq. (7). If the lifting surface or surfaces are synthesized from a large number of horseshoe vortices, each covering a small spanwise increment of one lifting surface, we can approximate the aerodynamic force as being constant over each spanwise increment. Then, from Eq. (7), the total aerodynamic force is given by

$$\boldsymbol{F} = \rho \sum_{i=1}^N \left(\Gamma_i \boldsymbol{V}_\infty + \sum_{j=1}^N \frac{\Gamma_i \Gamma_j}{\bar{c}_j} \boldsymbol{v}_{ji} \right) \times \delta \boldsymbol{\ell}_i \tag{24}$$

where $\delta \boldsymbol{\ell}_i$ is the spatial vector along the bound segment of horseshoe vortex i from node 1 to node 2, in the direction of segment vorticity. When we nondimensionalize Eq. (24), the total nondimensional aerodynamic force is

$$\frac{\boldsymbol{F}}{\frac{1}{2}\rho V_\infty^2 A_r} = 2 \sum_{i=1}^N \left(G_i \boldsymbol{v}_\infty + \sum_{j=1}^N G_i G_j \boldsymbol{v}_{ji} \right) \times \boldsymbol{\zeta}_i \frac{\delta A_i}{A_r} \tag{25}$$

where δA_i is the planform area of segment i,

$$\delta A_i = \int_{s=s_1}^{s_2} c \, \mathrm{d}s \tag{26}$$

The aerodynamic moment generated about the center of gravity is

$$\boldsymbol{M} = \rho \sum_{i=1}^N \boldsymbol{r}_i \times \left[\left(\Gamma_i \boldsymbol{V}_\infty + \sum_{j=1}^N \frac{\Gamma_i \Gamma_j}{\bar{c}_j} \boldsymbol{v}_{ji} \right) \times \delta \boldsymbol{\ell}_i \right] + \delta \boldsymbol{M}_i \tag{27}$$

If we assume a constant section moment coefficient C_{mi} over each spanwise increment, then

$$\delta \boldsymbol{M}_i = -\frac{1}{2}\rho V_\infty^2 C_{mi} \int_{s=s_1}^{s_2} c^2 \, \mathrm{d}s \, \boldsymbol{u}_{si} \tag{28}$$

where $\boldsymbol{u}_{si}$ is the local spanwise unit vector shown in Fig. 3,

$$\boldsymbol{u}_{si} = \boldsymbol{u}_{ai} \times \boldsymbol{u}_{ni} \tag{29}$$

When we use Eq. (28) in Eq. (27) and nondimensionalize

$$\frac{\boldsymbol{M}}{\frac{1}{2}\rho V_\infty^2 A_r L_r} = \sum_{i=1}^N \left\{ 2\boldsymbol{r}_i \times \left[\left(G_i \boldsymbol{v}_\infty + \sum_{j=1}^N G_i G_j \boldsymbol{v}_{ji} \right) \times \boldsymbol{\zeta}_i \right] \right.$$
$$\left. - \frac{C_{mi}}{\delta A_i} \int_{s=s_1}^{s_2} c^2 \, \mathrm{d}s \, \boldsymbol{u}_{si} \right\} \frac{\delta A_i}{A_r L_r} \tag{30}$$

To this point, the local characteristic length $\bar{c}_i$ has not been defined. It could be any characteristic length associated with the spanwise increment of the lifting surface that is associated with horseshoe vortex i. From Eq. (30), we see that the natural choice for this local characteristic length is the integral of the chord length squared, with respect to the spanwise coordinate, divided by the incremental area. If we also assume a linear variation in chord length over each spanwise increment, we have

$$\delta A_i = \int_{s=s_1}^{s_2} c \, \mathrm{d}s = \frac{c_{i_1} + c_{i_2}}{2}\left(s_{i_2} - s_{i_1}\right) \tag{31}$$

and

$$\bar{c}_i \equiv \frac{1}{\delta A_i} \int_{s=s_1}^{s_2} c^2 \, \mathrm{d}s = \frac{2}{3}\frac{c_{i_1}^2 + c_{i_1} c_{i_2} + c_{i_2}^2}{c_{i_1} + c_{i_2}} \tag{32}$$

When we use these definitions in Eq. (30), the dimensionless aerodynamic moment about the c.g. is

$$\frac{\boldsymbol{M}}{\frac{1}{2}\rho V_\infty^2 A_r L_r} = \sum_{i=1}^N \left\{ 2\boldsymbol{r}_i \times \left[\left(G_i \boldsymbol{v}_\infty + \sum_{j=1}^N G_i G_j \boldsymbol{v}_{ji} \right) \times \boldsymbol{\zeta}_i \right] \right.$$
$$\left. - C_{mi} \bar{c}_i \boldsymbol{u}_{si} \right\} \frac{\delta A_i}{A_r L_r} \tag{33}$$

Once the N dimensionless vortex strengths G_i are known, Eqs. (25) and (33) are used to evaluate the aerodynamic forces and moments.

Like panel methods, lifting-line theory provides only a potential flow solution. Thus, the forces and moments computed from this method do not include viscous effects, so that the parasitic drag is unobtainable. In addition to this restriction, that also applies to panel methods, lifting-line theory imposes an additional restriction that does not apply to panel methods. For lifting surfaces with low aspect ratio, Prandtl's hypothesis breaks down, and the usual relationship between local section lift and local section angle of attack no longer applies. It has long been established that lifting-line theory gives good agreement with experimental data for lifting surfaces of aspect ratio greater than about four.[2] For lifting surfaces of lower aspect ratio, panel methods or CFD solutions should be used.
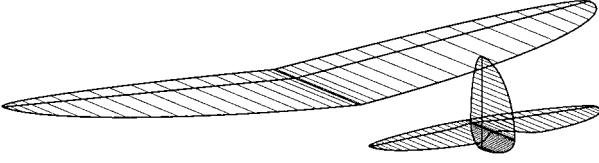
Fig. 4 Lifting-line grid with cosine clustering and 20 elements per semispan.

Grid Generation and Control Points

Each lifting surface must, of course, be divided into spanwise elements, in a manner similar to that shown symbolically in Fig. 1. In Fig. 1, the wing is divided into elements of equal spanwise increment. However, this is not the most efficient way in which to grid a lifting surface. Because vorticity is shed from a lifting surface more rapidly in the region near the tips, the nodal points should be clustered more tightly in this region for best computational efficiency. The authors have found conventional cosine clustering to be quite efficient. For straight lifting surfaces, clustering is only needed near the tips and the cosine distribution can be applied across the entire span. However, for a lifting surface with sweep and/or dihedral, there is a step change in the slope of the quarter chord at the root. This step change causes the downwash to change very rapidly in the region near the root. Thus, in general, the authors recommend applying cosine clustering independently over each semispan of each lifting surface, as shown in Fig. 4. This clusters the nodes more tightly at both the tip and the root. This clustering is based on the change of variables,

$$s/b = [1 - \cos(\phi)]/4 \qquad (34)$$

Over each semispan, ϕ varies from zero to π as s varies from zero to $b/2$. Distributing the nodes uniformly in ϕ will provide the desired clustering in s. If the total number of horseshoe elements desired on each semispan is n, the spanwise nodal coordinates are computed from,

$$s_i/b = \tfrac{1}{4}[1 - \cos(i\pi/n)], \qquad 0 \le i \le n \qquad (35)$$

where the bound segment of horseshoe vortex i extends from node i to node $i - 1$ on a left semispan and from node $i - 1$ to node i on a right semispan. The authors have found that using this nodal distribution with about 40 horseshoe elements per semispan gives the best compromise between speed and accuracy. Figure 4 shows a system of lifting surfaces overlaid with a grid of this type using 20 elements per semispan.

Because singularities occur at the junctures of adjacent bound-vortex segments, for maximum accuracy and computational efficiency, the location of control points must be critically assessed. At first thought, it would seem most reasonable to place control points on the bound segment of each vortex, midway between the two trailing legs. However, the authors have found that this does not give the best numerical accuracy. A significant improvement in accuracy, for a given number of elements, can be achieved by placing the control points midway in ϕ rather than midway in s. Thus, the spanwise control point coordinates are computed from

$$s_i/b = \tfrac{1}{4}\{1 - \cos[(i\pi/n) - (\pi/2n)]\}, \qquad 1 \le i \le n \qquad (36)$$

This distribution places control points very near the spatial midpoint of each bound vortex segment, over most of the wing. However, near the root and the tip, these control points are significantly offset from the spatial midpoint.

Results

For straight elliptic wings with no geometric twist and no aerodynamic twist, Prandtl's classical lifting-line theory gives a very simple and well-known closed-form solution. From this solution, the section lift distribution in the spanwise direction is given by

$$\frac{f_\ell}{\tfrac{1}{2}\rho V_\infty^2 \bar{c} C_{\ell\infty}} = \frac{4R_a}{\pi R_a + C_{\ell_\alpha}}[1 - (2s/b)^2]^{\frac{1}{2}} \qquad (37)$$
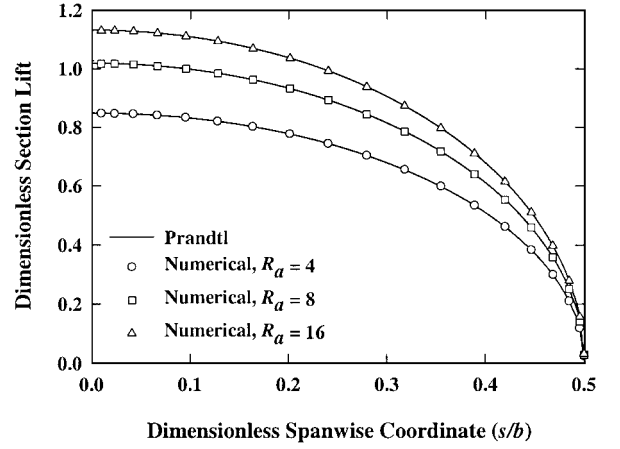

Fig. 5 Section lift distribution for three elliptic wings.
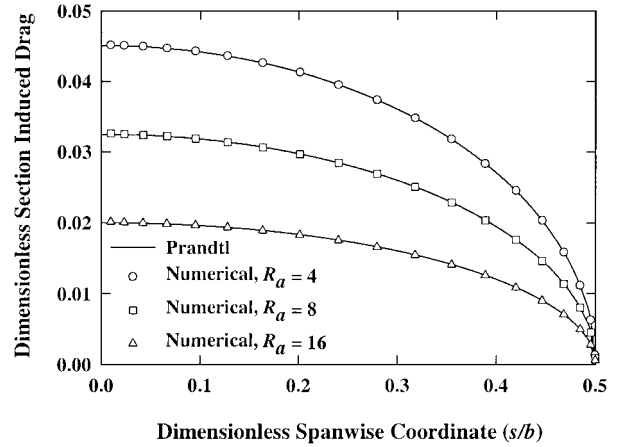

Fig. 6 Section induced drag distribution for three elliptic wings.

This same solution gives the local section induced drag

$$\frac{f_{d_i}}{\tfrac{1}{2}\rho V_\infty^2 \bar{c} C_{\ell\infty}^2} = \frac{4R_a}{\left(\pi R_a + C_{\ell_\alpha}\right)^2}[1 - (2s/b)^2]^{\frac{1}{2}} \qquad (38)$$

As a first-order test, the numerical method presented here should agree with Eqs. (37) and (38), at small angles of attack, for a straight elliptic wing with no geometric or aerodynamic twist. Figure 5 shows a comparison between the section lift distribution predicted by Eq. (37) and that predicted by the present numerical method for three straight elliptic wings of different aspect ratio. Figure 6 compares the induced drag distribution predicted by Eq. (38) to that predicted from the present method for the same three elliptic wings. A similar comparison for tapered wings shows very similar results. The numerical results shown in Figs. 5 and 6 were all generated using 40 horseshoe elements per semispan for wings having a NACA 2412 airfoil section. Similar comparisons were made for other straight wings having varying amounts of camber, taper, and washout. Camber was varied from 0 to 8%, taper ratio was varied from 0.1 to 1.0, and washout was varied from 0 to 5 deg. In all cases, the numerical solution using 40 horseshoe elements per semispan agreed with the classical lifting-line solution to within two-tenths of 1% for the induced drag and to within five-hundredths of 1% for the lift. Thus, for all practical purposes, results obtained from this numerical lifting-line method are identical to those obtained from the classical lifting-line solution for a single lifting surface with no sweep or dihedral. Because, for straight wings of aspect ratios greater than about four, the classical solution is known to adequately predict the effects of aspect ratio, camber, and planform shape, the same can be said for the present numerical solution.

Unlike the analytical solution to Prandtl's classical lifting-line theory, the present numerical method can be applied to wings with

sweep and/or dihedral. To examine how well the present method predicts the effects of sweep and dihedral, results obtained from this method were compared with results obtained from a numerical panel method and from an inviscid CFD solution. The results predicted for the effects of sweep were also compared with limited experimental data.

For the numerical panel method comparison, the commercial code PMARC[18,19] was selected. This code was developed at NASA Ames Research Center and is one of the most efficient numerical panel codes available. PMARC uses flat quadrilateral panels with uniform source and doublet distributions on each panel. This code also accounts for the effects of wake rollup, using an unsteady wake development approach.

The commercial code WIND,[20] developed by the NPARC Alliance, was chosen for the inviscid CFD comparison. This code uses a node-centered finite volume approach to solve the Euler equations on a structured grid. The available fifth-order upwind-biased discretization scheme was used to reduce the effects of numerical viscosity.

For all three numerical methods the grid size was repeatedly refined until the solution was no longer significantly affected by further grid refinement. By this procedure, an optimum grid for each of the three methods was selected as that which gave the best combination of accuracy and computational speed. With this method of grid resolution, the numerical lifting-line method required 40 section elements per semispan. Grid-resolved solutions for PMARC required 4500 panels per semispan. The selected grid was partitioned to give 45 segments along the semispan and 90 around the circumference, with panels clustered near the leading edge, the trailing edge, and the wingtips. For WIND, a two-block H–H type mesh with 1.25×10^6 grid points per semispan gave the best compromise between accuracy and computational efficiency. The computational domain for the WIND solutions extended approximately 30 chords from the wing in all directions, with grid points clustered near the wing and the trailing-tip vortices. When these resolved grids were used for the three methods, the computational time required to obtain a solution from PMARC was about 2×10^4 times that required using the present numerical lifting-line method. The WIND solutions required approximately 2×10^6 times as long as the lifting-line solutions.

A comparison between results obtained from these three numerical methods and previously published experimental data is shown in Figs. 7 and 8. The solid lines and filled symbols correspond to a straight wing of aspect ratio 6.57, with experimental data obtained from McAlister and Takahashi.[21] The dashed lines and open symbols are for a 45-deg swept wing of aspect ratio 5.0, having experimental data reported by Weber and Brebner.[22] Both wings have symmetrical airfoil sections with no geometric twist and constant chord throughout the span. The straight wing has a thickness of 15% and the swept wing has a thickness of 12%.

Fig. 8   Comparison between the induced drag coefficient predicted by the numerical lifting-line method, PMARC, and WIND with that obtained from experimental data, for a straight wing and a wing with 45 deg of sweep.

From the results shown in Fig. 7, we see that the lift coefficient predicted by all three methods is in good agreement with experimental observations for both wings. From Fig. 8 we see that, for the straight wing, the induced drag predicted by both the numerical lifting-line method and by PMARC is in good agreement with experimental data, whereas WIND gives an induced drag that is somewhat higher. The predictions for induced drag on the swept wing are not nearly as good. For this wing, the induced drag predicted by the panel code is about 40% less than that observed experimentally. However, both the numerical lifting-line method and the CFD solution give induced drag values that are about 25% above the experimental values. Still, the values of induced drag predicted by the numerical lifting-line method are as good as or better than those predicted by the other two methods, even for this highly swept wing. Furthermore, the induced drag on a highly swept wing, as predicted by the present method, appears to be somewhat conservative, whereas the panel code predicts an induced drag that is too low. Though none of the numerical methods tested seemed to do very well at predicting the effects of sweep on induced drag, all three of the methods appeared to do a good job of predicting the effects of sweep on lift.

To obtain the numerical lifting-line solutions shown in Figs. 7 and 8, we have used the linear relationship between a two-dimensional section lift coefficient and a section angle of attack that is predicted by thin airfoil theory. Because the downwash and induced angle of attack are obtained from the solution to the nonlinear system given by Eq. (11), we have no reason to expect that the lift coefficient predicted for the complete wing should be a linear function of geometric angle of attack. However, the results in Fig. 7 show that this relationship is, in fact, very nearly linear for both wings. The result predicted for the straight wing is almost exactly linear, as is also predicted by the classical lifting-line solution. Even for the highly swept wing, the deviation from linearity is quite small. Both the panel code and the experimental data confirm this result.

The overprediction of induced drag by the CFD code for both the straight wing and the swept wing is likely due to numerical viscosity and is expected. However, the reason that the numerical lifting-line method overpredicts induced drag for the swept wing, but not for the straight wing, may be less obvious. The foundation of lifting-line theory requires the bound vorticity to follow the chordwise aerodynamic center of the wing. The numerical lifting-line solution shown in Fig. 8 was obtained by assuming that the lifting-line follows the wing quarter chord, which is the theoretical aerodynamic center from thin airfoil theory. With this assumption, the discontinuity in the slope of the quarter chord at the spanwise midpoint of a highly swept wing produces a rather strong singularity (see, for example, Cheng and Meng[23]). This results in the prediction of strong downwash and large induced drag in the region near this singularity. In reality, the experimental results of Weber and Brebner[22] show that,
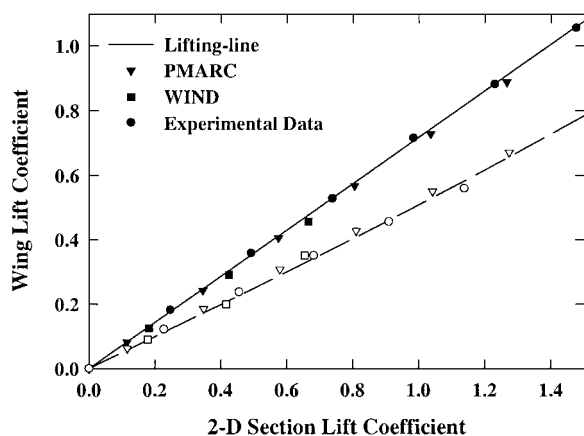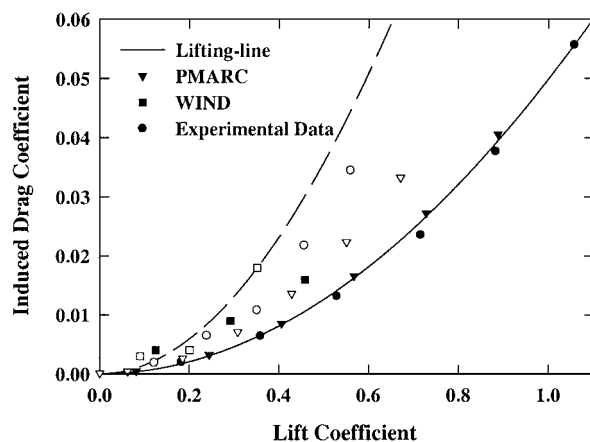

Fig. 7   Comparison between the lift coefficient predicted by the numerical lifting-line method, PMARC, and WIND with that obtained from experimental data, for a straight wing and a wing with 45 deg of sweep.
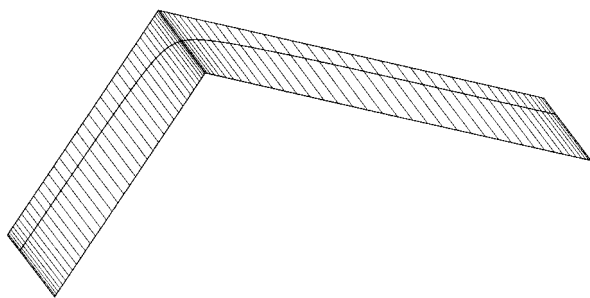
Fig. 9 Deviation of the aerodynamic center from the quarter chord in the region near the spanwise midpoint of a highly swept wing.
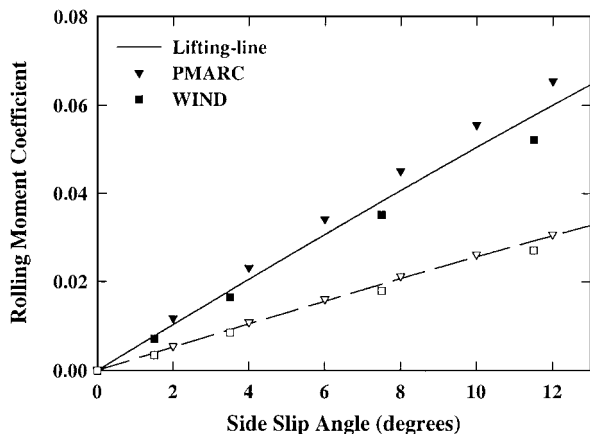

Fig. 10 Comparison between the rolling moment coefficient predicted by the numerical lifting-line method, PMARC, and WIND for wings with 10 and 20 deg of dihedral.

Fig. 11 Pressure forces and shed vorticity for a system of lifting surfaces as predicted by the numerical lifting-line method.

near the spanwise midpoint of a highly swept wing, the aerodynamic center moves considerably aft of the wing quarter chord, as shown in Fig. 9. This removes the discontinuity in slope at the spanwise midpoint of the lifting line and significantly reduces the predicted induced drag. Unfortunately, there is currently no simple means to predict the true chordwise aerodynamic center of a highly swept wing in the region near the spanwise midpoint. Thus, the present method cannot easily be corrected to remove this error.

The accuracy of the present numerical lifting-line method for predicting dihedral effects was also tested by comparing this method with both PMARC and WIND. Figure 10 shows the variation in rolling moment coefficient with sideslip angle for two nonplanar rectangular wings having different dihedral, as predicted by all three methods. Both wings have symmetric NACA 0015 airfoil sections with no sweep or twist and an aspect ratio of 6.57. The solid line and filled symbols correspond to a wing with 20 deg dihedral, whereas the dashed line and open symbols are for a wing with 10 deg dihedral.

From Fig. 10, we see that all three methods agree very closely in their predictions for the wing with 10 deg dihedral. For this wing the agreement between the lifting-line method and the panel code is within 2%, and the CFD solution agrees with the lifting-line solution to within 7%. The three methods do, however, diverge somewhat in their predictions for the wing with 20-deg dihedral. This divergence becomes more pronounced at very large sideslip angles. For the wing with 20-deg dihedral at sideslip angles in the range of 12 deg, the panel code predicts a rolling moment coefficient that is about 9% above that predicted by the lifting-line method, whereas the CFD solution predicts a result that is nearly 10% below the lifting-line solution.

The present numerical method could be used to predict the aerodynamic forces and moments acting on a system of lifting surfaces with arbitrary position and orientation. Each lifting surface would be synthesized by distributing horseshoe vortices on a grid structured similarly to that shown in Fig. 4. Because all of the horseshoe vortices used to synthesize the complete system of lifting surfaces
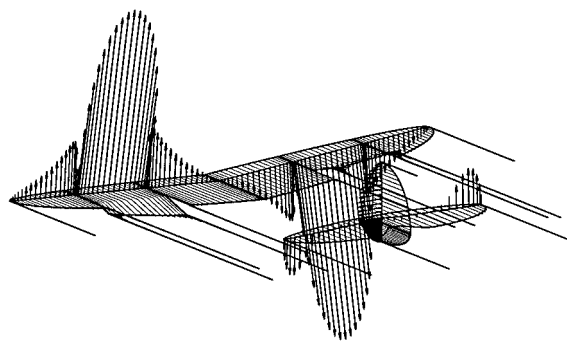
are combined and forced to satisfy Eq. (11) as a single system of coupled equations, the interactions between lifting surfaces are directly accounted for. An example of such interactions can be seen in Fig. 11. The lifting surfaces shown in Fig. 11 all have symmetric airfoil sections and are oriented to give a zero geometric angle of attack. The only direct production of lift in this configuration comes from a deflection of the ailerons. The deflected ailerons produce lift and vorticity that in turn induce lift and vorticity on all other surfaces. In Fig. 11 the arrows indicate the magnitude and direction of the local section force, and the streamwise lines at the trailing edge of each lifting surface indicate the magnitude of the local shed vorticity. As can be seen from Fig. 11, the lifting surface interactions predicted by the present method are at least qualitatively correct. However, further study is needed to determine the quantitative accuracy of the predicted lifting surface interactions.

The present numerical method contains no inherent requirement for a linear relationship between section lift and section angle of attack. Thus, the method could conceivably be applied, with caution, to account approximately for the effects of stall. The lifting-line method requires a known relationship for the section lift coefficient as a function of section angle of attack. Because such relationships must be obtained experimentally beyond stall, the present method would predict stall by using a semi-empirical correction to an otherwise potential flow solution. For this reason, the method should be used with extreme caution for angles of attack beyond stall. However, the method may be able to predict the onset of stall. Further study is needed to determine to what extent the method can be used at angles of attack near or beyond stall.

Conclusions

The insight of Ludwig Prandtl (1875–1953) was nothing short of astonishing. This was never more dramatically demonstrated than in the development of his classical lifting-line theory, during the period from 1911–1918. The utility of this simple and elegant theory is so great that it is still widely used today. Furthermore, with a few minor alterations and the use of a modern computer, the model proposed by Prandtl can be used to predict the inviscid forces and moments acting on lifting surfaces of aspect ratio greater than about four with an accuracy as good as that obtained from modern panel codes or CFD, but at a small fraction of the computational cost.

References

[1]Prandtl, L., "Tragflügel Theorie," *Nachrichten von der Gesellschaft der Wisseschaften zu Göttingen*, Geschäeftliche Mitteilungen, Klasse, 1918, pp. 451–477.

[2]Prandtl, L., "Applications of Modern Hydrodynamics to Aeronautics," NACA 116, June 1921.

[3]Kutta, M. W., "Auftriebskräfte in Strömenden Flüssigkeiten," *Illustrierte Aeronautische Mitteilungen*, Vol. 6, 1902, p. 133.

[4]Joukowski, N. E., "Sur les Tourbillons Adjionts," *Traraux de la Section Physique de la Societe Imperiale des Amis des Sciences Naturales*, Vol. 13, No. 2, 1906.

[5]Bertin, J. J., and Smith, M. L., "Incompressible Flow About Wings of Finite Span," *Aerodynamics for Engineers*, 3rd ed., Prentice–Hall, Upper Saddle River, NJ, 1998, pp. 261–336.

[6]Saffman, P. G., "Vortex Force and Bound Vorticity," *Vortex Dynamics*, Cambridge Univ. Press, Cambridge, England, U.K., 1992, pp. 46–48.

[7]Glauert, H., *The Elements of Aerofoil and Airscrew Theory*, 2nd ed., Cambridge Univ. Press, Cambridge, England, U.K., 1959, pp. 142–145.

[8]Multhopp, H., "Die Berechnung der Auftriebs Verteilung von Tragflugeln," *Luftfahrtforschung*, Vol. 15, No. 14, 1938, pp. 153–169.

[9]Rasmussen, M. L., and Smith, D. E., "Lifting-Line Theory for Arbitrary Shaped Wings," *Journal of Aircraft*, Vol. 36, No. 2, 1999, pp. 340–348.

[10]Lotz, I., "Berechnung der Auftriebsverteilug beliebig geformter Flugel," *Zeitschrift für Flugtechnik und Motorluftschiffahrt*, Vol. 22, No. 7, 1931, pp. 189–195.

[11]Karamcheti, K., "Elements of Finite Wing Theory," *Ideal-Fluid Aerodynamics*, Wiley, New York, 1966, pp. 535–567.

[12]McCormick, B. W., "The Lifting Line Model," *Aerodynamics, Aeronautics and Flight Mechanics*, 2nd ed., Wiley, New York, 1995, pp. 112–119.

[13]Anderson, J. D., Jr., Corda, S., and Van Wie, D. M., "Numerical Lifting-Line Theory Applied to Drooped Leading-Edge Wings Below and Above Stall," *Journal of Aircraft*, Vol. 17, No. 12, 1980, pp. 898–904.

[14]Katz, J., and Plotkin, A., "Lifting-Line Solution by Horseshoe Elements," *Low-Speed Aerodynamics, from Wing Theory to Panel Methods*, McGraw–Hill, New York, 1991, pp. 379–386.

[15]Katz, J., and Plotkin, A., "Constant-Strength Vortex Line Segment," *Low-Speed Aerodynamics, from Wing Theory to Panel Methods*, McGraw–Hill, New York, 1991, pp. 291–294.

[16]Falkner, V. M., "The Calculation of Aerodynamic Loading on Surfaces of Any Shape," *Reports and Memoranda 1910*, Aeronautical Research Council, London, Aug. 1943.

[17]Multhopp, H., "Method for Calculating the Lift Distribution of Wings (Subsonic Lifting Surface Theory)," *Reports and Memoranda 2884*, Aeronautical Research Council, London, Jan. 1950.

[18]Katz, J., and Maskew, B., "Unsteady Low-Speed Aerodynamics Model for Complete Aircraft Configurations," *Journal of Aircraft*, Vol. 25, No. 4, 1988, pp. 302–310.

[19]Ashby, D. L., Dudley, M. R., and Iguchi, S. K., "Development and Validation of an Advanced Low-Order Panel Method," NASA TN-101024, Oct. 1988.

[20]Bush, R. H., Power, G. D., and Towne, C. E., "WIND: The Production Flow Solver of the NPARC Alliance," AIAA Paper 98-0935, Jan. 1998.

[21]McAlister, K. W., and Takahashi, R. K., "NACA 0015 Wing Pressure and Trailing Vortex Measurements," NASA TP-3151, Nov. 1991.

[22]Weber, J., and Brebner, G. G., "Low-Speed Tests on 45-deg Swept-Back Wings, Part I: Pressure Measurements on Wings of Aspect Ratio 5," *Reports and Memoranda 2882*, Aeronautical Research Council, London, May 1958.

[23]Cheng, H. K., and Meng, S. Y., "The Oblique Wing as a Lifting-Line Problem in Transonic Flow," *Journal of Fluid Mechanics*, Vol. 97, No. 3, 1980, pp. 531–556.